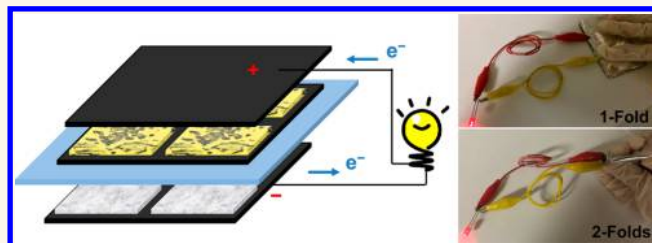


# A Foldable Lithium–Sulfur Battery

Lu Li,<sup>†</sup> Zi Ping Wu,<sup>§</sup> Hao Sun,<sup>||</sup> Deming Chen,<sup>§</sup> Jian Gao,<sup>‡</sup> Shravan Suresh,<sup>†</sup> Philippe Chow,<sup>‡</sup> Chandra Veer Singh,<sup>||, #</sup> and Nikhil Koratkar<sup>\*, †, ‡</sup>

<sup>†</sup>Mechanical, Aerospace and Nuclear Engineering, and <sup>‡</sup>Materials Science and Engineering, Rensselaer Polytechnic Institute, 110 8th Street, Troy, New York 12180, United States, <sup>§</sup>Jiangxi Key Laboratory of Power Battery and Materials, School of Materials Science and Engineering, Jiangxi University of Science and Technology, 86 Hong Qi Road, Ganzhou 341000, P. R. China, <sup>||</sup>Department of Mechanical and Industrial Engineering, University of Toronto, 5 King's College Road, Toronto M5S 3G8, Ontario, Canada, and <sup>#</sup>Department of Materials Science and Engineering, University of Toronto, 184 College St, Suite 140, Toronto M5S 3E4, Ontario, Canada

**ABSTRACT** The next generation of deformable and shape-conformable electronics devices will need to be powered by batteries that are not only flexible but also foldable. Here we report a foldable lithium–sulfur (Li–S) rechargeable battery, with the highest areal capacity ( $\sim 3 \text{ mAh cm}^{-2}$ ) reported to date among all types of foldable energy-storage devices. The key to this result lies in the use of fully foldable and superelastic carbon nanotube current-collector films and impregnation of the active materials (S and Li) into the current-collectors in a checkerboard pattern, enabling the battery to be folded along two mutually orthogonal directions. The carbon nanotube films also serve as the sulfur entrapment layer in the Li–S battery. The foldable battery showed <12% loss in specific capacity over 100 continuous folding and unfolding cycles. Such shape-conformable Li–S batteries with significantly greater energy density than traditional lithium-ion batteries could power the flexible and foldable devices of the future including laptops, cell phones, tablet computers, surgical tools, and implantable biomedical devices.



**KEYWORDS:** foldable battery · lithium–sulfur battery · shape conformality · carbon nanotubes

The next great innovation in the portable electronics and communication devices sector is expected to be fully shape conformable and wearable devices. Some examples of such deformable prototype concepts include the Philips Fluid Flexible Smart-Phone, Samsung Flexible Prototype Display Windows, and the iPhone ProCare.<sup>1</sup> However, it should be noted that such flexible and foldable electronics devices can function only if the energy source that is powering it is also designed to be equally flexible and foldable.

While many flexible battery and supercapacitor devices have been reported in the literature, there are very few reports of “foldable” energy storage devices. A few groups have reported foldable lithium-ion batteries (LIBs)<sup>2–4</sup> featuring carbon nanotube (CNT) macropaper as the current collectors. Highly stretchable and foldable supercapacitors using CNT cables have also been reported;<sup>5</sup> however, to our knowledge there is no report so far of a foldable lithium–sulfur (Li–S) battery. A Li–S rechargeable battery has a theoretical capacity of  $\sim 1675 \text{ mAh g}^{-1}$  (energy density of  $\sim 2600 \text{ Wh kg}^{-1}$ ),<sup>6</sup> which is much higher

than that of LIBs ( $\sim 387 \text{ Wh kg}^{-1}$  for typical  $\text{LiCoO}_2/\text{graphite}$  system)<sup>7</sup> and supercapacitors ( $\sim 10 \text{ Wh kg}^{-1}$ ).<sup>8</sup> A Li–S configuration could therefore prove to be a very promising candidate in realizing high energy density foldable batteries.

Why is it so challenging to design a foldable battery? There are two principal reasons for this: (1) metal current collectors (such as aluminum (Al) or copper (Cu) foils) onto which the active material is pasted cannot be folded as they undergo plastic deformation when folded, and (2) the active material (such as graphitic slurry or lithium cobalt oxide slurry) easily delaminates (*i.e.*, detaches) from the surface of the current collector or fractures when it is folded. Our solution to the first challenge is to replace metal current collectors with CNT films. In fact, we use multiple CNT current collector films to sandwich and entrap the sulfur in the cathode of our Li–S battery. While use of CNT films<sup>2–4</sup> as current collectors is not new, there is so far no clear understanding as to why CNT films can be successfully folded without plastic deformation. The ability of CNT films to be folded is surprising, since molecular dynamics (MD) simulations<sup>9,10</sup>

\* Address correspondence to koratn@rpi.edu.

Received for review August 14, 2015 and accepted September 27, 2015.

Published online  
10.1021/acsnano.5b05068

© XXXX American Chemical Society

indicate that an individual CNT while fully elastic at bend angles of up to  $\sim 120^\circ$ , will deform plastically and break at bend angles close to  $\sim 180^\circ$  which would be the case when the CNT is folded. In this work, using detailed MD simulations of individual CNT and CNT networks, we provide fundamental insight into why networks of interconnected CNTs are able to withstand the high stresses associated with folding without significant plastic deformation. The simulation results provide insight into how CNT films can be engineered to replace traditional metal foils as superelastic and fully foldable current collectors.

Our solution to the second challenge (delamination and fracture of the active material) is to impregnate the active materials (sulfur and lithium in this case) in a checkerboard pattern. It should be noted that while foldability of the cathode (sulfur part) has been realized by combining sulfur with various foldable current collectors,<sup>11–13</sup> the plasticity of the Li metal during the folding/unfolding process is the main obstacle to achieving a foldable Li–S battery. In our design, the use of a checkerboard pattern means that the Li does not form a continuous film and the folding takes place predominantly in the pure CNT region (without Li or S). The active material deposited in the checkerboard pattern is therefore far less prone to delamination and fracture. The checkerboard pattern establishes the two principal (*i.e.*, mutually orthogonal) directions along which the battery can be folded. Such foldability along two principal directions is sufficient for the successful folding of portable electronics devices such as cellular phones and tablet computers. In spite of the aforementioned patterning of the active materials, we are still able to maintain a relatively high mass loading of sulfur ( $\sim 3.6 \text{ mg cm}^{-2}$  in the folded state) resulting in an areal capacity of  $\sim 3 \text{ mAh cm}^{-2}$  (in a pouch cell configuration). This is several-fold higher than previously reported foldable<sup>2–4</sup> and flexible<sup>14–18</sup> lithium-ion batteries which exhibit capacities in the range of  $0.1\text{--}1.5 \text{ mAh cm}^{-2}$ . Our Li–S battery device could be successfully folded and unfolded over 100 times with only  $\sim 12\%$  loss in the areal capacity. This work demonstrates the feasibility of developing foldable Li–S batteries and could open the door to their use in next generation, shape-conformable, and wearable electronics and communication devices.

## RESULTS AND DISCUSSION

**Foldability of CNT Current Collector.** Free-standing (*i.e.*, self-supporting) CNT films were prepared (Figure 1a) *via* floating catalyst chemical vapor deposition (FC-CVD) as shown in our previous work.<sup>19</sup> The FC-CVD process shows promise for scalable manufacturing of CNT films for industrial scale applications. The CNT film exhibits a high electrical conductivity of  $\sim 800 \text{ S cm}^{-1}$  (Supporting Information Figure S1). It is highly lightweight and thin ( $0.6\text{--}0.8 \text{ mg cm}^{-2}$ ,  $\sim 3 \mu\text{m}$  thick) when

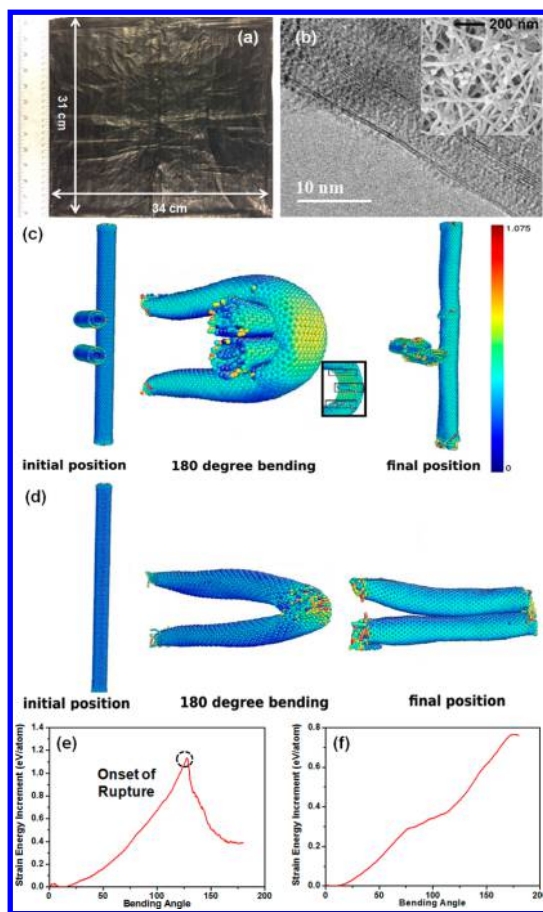


**Figure 1.** Superelastic and foldable carbon nanotube current collectors: (a) Photograph of free-standing, large-area carbon nanotube film. (b) Transmission electron micrograph indicating that the nanotubes in the film are predominantly double walled (DWCNT); inset shows scanning electron microscopy imaging of the film indicating a cross-linked (interconnected), porous network of nanotubes. (c, d) Molecular dynamics (MD) simulations of folding of carbon nanotube network; snapshots of folding process for three DWCNTs system is shown in (c) and single DWCNT is shown in (d). In panel (c), the small figure in the black rectangle shows the back side of the bending point for three DWCNT system (only the bent DWCNT is shown). The bulges formed during bending are labeled by small black rectangles. The different colors are a representation of different atomistic strain, and the color map is labeled on the right. (e) Relation between strain energy increment vs bending angle for single DWCNT system. (f) Relation between strain energy increment vs bending angle for three DWCNT system (only the energy of the bended DWCNT is calculated).

compared with typical aluminum (Al) foils ( $\sim 5.6 \text{ mg cm}^{-2}$ ,  $\sim 15 \mu\text{m}$  thick), and much more chemically stable than Al foils which are prone to metal corrosion during cycling.<sup>20</sup> Therefore, compared to the conventional Al foil current collector, improved lithium ion diffusion kinetics, lower polarization, and higher gravimetric energy densities of the electrodes could be expected when employing CNT films as the current collectors. The inset in Figure 1b shows scanning electron microscopy (SEM) imaging of the carbon nanotube bundles (or ropes) that comprise the CNT film. The nanotube bundles are cross-linked and form an interconnected

three-dimensional porous network structure. Transmission electron microscopy (TEM) imaging (a representative micrograph is provided in Figure 1b) revealed that the majority of the nanotubes in the bundles are double walled carbon nanotubes (DWCNTs).

The CNT film exhibited superelastic behavior and sprung back to its original shape even after repeated folding of the film. This behavior is surprising since the literature<sup>9,10,21–24</sup> indicates that while an individual CNT is highly elastic, it cannot be folded (*i.e.*, bent at an angle of 180°). The underlying atomistic mechanism by which the CNT film could be folded and refolded multiple times without significant plastic deformation is not known. To better understand the origin of the superelasticity in the CNT film we performed molecular dynamics (MD) simulations of bending of individual DWCNT as well as networks of cross-linked DWCNTs (as in Figure 1b). TEM analysis of the CNT film (Figure 1b), indicates that the film is comprised primarily of DWCNTs that are agglomerated into ropes that form an interconnected (cross-linking) network. The smallest building block of the carbon nanotube paper is therefore the DWCNT. Hence we used DWCNT in our simulation work. Previous simulations have suggested that individual single walled CNT can be bent elastically up to a bending angle  $\theta \leq 120^\circ$ , beyond which the covalent bond between carbon atoms will break and irreversible plastic deformation is ensued.<sup>9,10</sup> However, it should be noted that previous investigations<sup>9,10,21–24</sup> have been focused on single CNTs, and not on the deformation response of interconnected (cross-linked) networks of CNTs.

Two specific configurations were studied to identify and understand the interaction of different CNTs undergoing folding process. In the first configuration, bending deformation of an isolated DWCNT was studied, as this represents the case when the nanotubes in the film are oriented in a single direction parallel to each other. The second configuration consisted of three DWCNTs with two oriented in one direction, and the third one oriented normal to the other two. The CNT film in our experiments has a cross-linked network structure of DWCNTs with diameter of  $\sim 5$  nm, supported solely by van der Waals forces. From the experimental micrograph depicted in Figure 1b, different parallel DWCNTs aggregate to form a nanotube bundle and different such bundles are interconnected with each other. During the folding process, all nanotubes in the bending bundles are deformed synchronously, so one single nanotube in a periodic super cell is analogous to the whole bundle. The bundles that are cross-linked with the bending DWCNT will in turn get sandwiched and squeezed. In order to simulate such a system, we placed two parallel DWCNTs situated perpendicular to the bending one. Please refer to the Supporting Information for the detailed model structure and the method of load application (Supporting Information Figures S2–S5).

Figure 1c,d depicts MD snapshots of the folding process. The strain of single DWCNT is concentrated in a narrow region at the bending point, while in the three-DWCNTs system it distributes more uniformly. The single DWCNT breaks at the point of bending (Figure 1d), while the three-DWCNT cross-linked configuration could reorient to the original position when unloaded (Figure 1c). It is the two cross-linking DWCNTs that play an important role herein. The bending area of the three-DWCNTs system deforms continually as a semicircle, without a sharp bending curvature as in the single DWCNT case. This semicircle formation decreases the magnitude of maximum strain by  $\sim 40\%$  (Figure 1c). For single DWCNT, all the atoms in the bending region are highly deformed (Figure 1d) with each atom preferring a random position. Such a highly disordered structure causes an agglomeration of strain energy at the highly stressed region, which leads to bond breaking. On the contrary, atoms in the bending region of three DWCNTs preserve the original hexagonal network (Figure 1c) with no bond breaking or disordered structure. The preservation of original periodic structure and decrease of atomistic strain are the two major reasons for the elastic folding. In other words the constraint imposed by the cross-linking tubes in limiting the maximum bend angle of the CNT plays a crucial role in enabling elastic folding. When only one DWCNT lies in the middle (Supporting Information Figure S4), the bending strain is also reduced when compared to the non cross-linked system, but not enough for it to recover completely.

For understanding the energetics of bending, we calculated the increment of strain energy per atom relative to the initial structure and recorded them in Figure 1e for the single nanotube and in Figure 1f for the three nanotube system. At lower bending angles,  $\theta < 60^\circ$ , a quadratic relation with respect to bending angle (or equivalently the elastic strain) signifying harmonic deformation is observed for both systems, which is consistent with linear elasticity. At larger bending angles, nonlinear local bulking begins and the strain energy exhibits more or less linear relationship with the bending angle. Subsequent deformation is primarily controlled by the change of carbon–carbon bond angle, rather than the bond length, consistent with previous observations.<sup>21,22</sup> In general, the three-DWCNTs case shows a much broader harmonic deformation region as well as a much lower maximum increment of strain energy per atom ( $\sim 18$  kcal mol<sup>-1</sup> or  $\sim 0.78$  eV) compared to the case of the single DWCNT ( $\sim 27.2$  kcal mol<sup>-1</sup> or  $\sim 1.18$  eV). This shows that although the three-DWCNT system undertakes 180° bending (*i.e.*, complete folding), the cross-linking of nanotubes decreases the energy increment significantly. These results suggest that increasing the density of cross-links is beneficial to suppressing plastic deformation in the network.

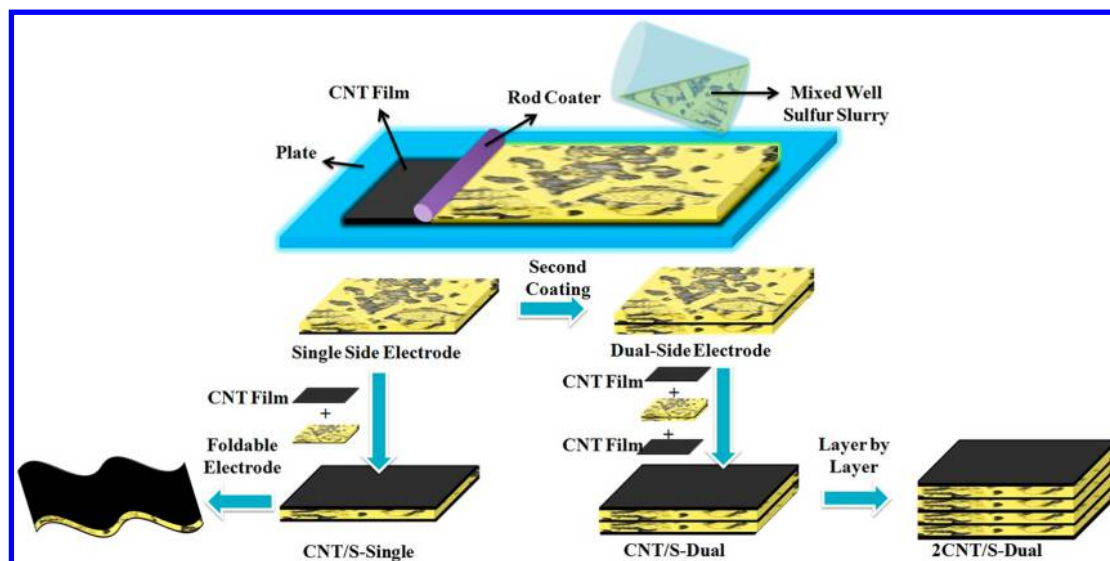


**Figure 2.** Sulfur–CNT composite cathode. Schematic of the electrode preparation process and the designed configurations. The CNT films serve as both the current collector and the sulfur entrapment layer. Depending on the number of sulfur and CNT layers, we produce three types of electrodes denoted in the schematic as CNT/S-Single, CNT/S-Dual, and 2CNT/S-Dual.

The large change in slope in Figure 1e (at bend angle of  $\sim 130^\circ$ ) for the single DWCNT folding case is due to onset of bond breakage and rupture. To summarize the above discussion, we find that the inherent hierarchical structure of the CNT film enables elastic folding. During folding, the cross-linked arrangement of CNT effectively decreases the overall bending deformation to around 40% in comparison to single CNT undergoing folding process. Consequently, upon unloading, the CNTs are found to recover back elastically. This explains why the CNT paper can be folded successfully without severe plastic deformation.

**Sulfur Electrode Fabrication and Characterization.** Figure 2 shows the preparation process and the design of the sulfur containing cathode. A well-mixed sulfur slurry was coated on the surface of the CNT film by the doctor-blade coating method shown schematically in Figure 2. We place another pure CNT film on the top of the sulfur-coated CNT electrode to form a sandwich structure electrode (denoted as CNT/S-Single with sulfur loading of  $\sim 1.8 \text{ mg cm}^{-2}$ ). The CNT films that encapsulate the sulfur layer function as both traditional current collectors, but also as sulfur reservoirs and barrier (*i.e.*, sulfur trapping) layers which is important for the electrochemical stability<sup>25,26</sup> of the Li–S battery. Further, as opposed to rigid metal current collectors, the CNT films can also buffer the large volumetric expansion of sulfur during the cycling process. We also explored variations of the above approach to further increase the mass loading of sulfur in the electrode. For example, we coated sulfur on both sides of a CNT film and sandwiched this structure between two additional CNT films (denoted as CNT/S-Dual in Figure 2 with sulfur loading of  $\sim 3.4 \text{ mg cm}^{-2}$ ). Finally, we designed a very high sulfur loading electrode configuration by stacking two dual-side sulfur coated CNT film

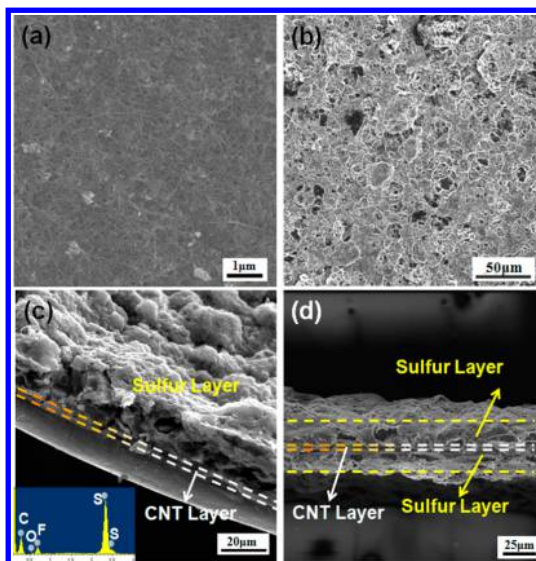


**Figure 3.** Morphologies and elemental analysis of the sulfur–CNT composite cathodes. (a) Scanning electron microscopy (SEM) image of the surface of the CNT film. (b) SEM image of the surface of the sulfur coated CNT film electrode. (c) Cross section of single side sulfur coated CNT film electrode and its corresponding EDS spectrum (inset of panel c; unit, keV). (d) Cross section of the dual-side sulfur coated CNT film electrode.

electrodes with one pure CNT film inserted between them and an additional two pure CNT films at the top and bottom (denoted as 2CNT/S-Dual in Figure 2 with a sulfur loading of  $\sim 6.8 \text{ mg cm}^{-2}$ ).

Figure 3b displays a SEM image of the single side sulfur-coated CNT film surface. The baseline CNT electrode prior to the sulfur coating is shown in Figure 3a. The slurry formed a homogeneous and compact layer on the CNT film. The presence of elemental C, O, S, and F (from the PVDF slurry) and their distributions were investigated using energy-dispersive X-ray (EDS)

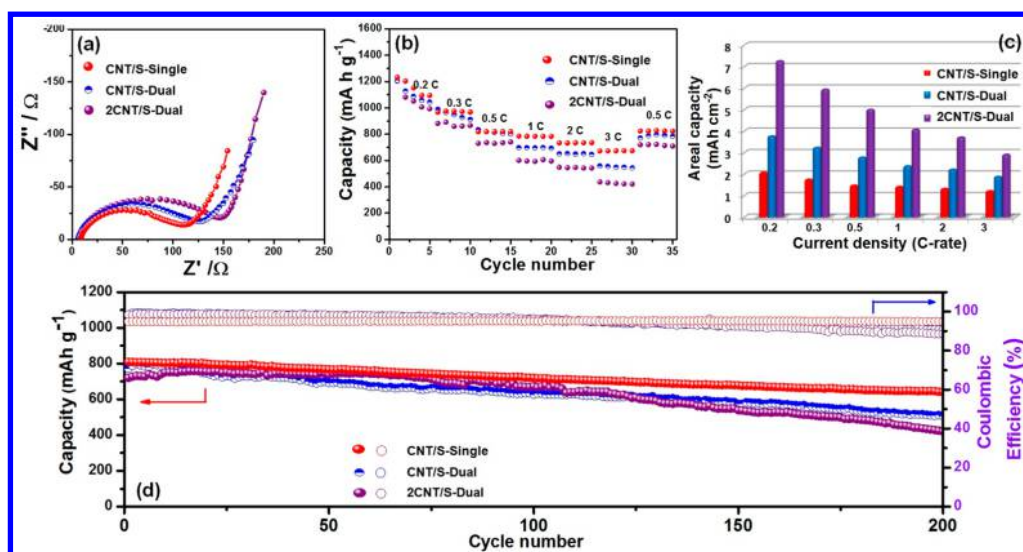


**Figure 4.** Electrochemical performance of Li–S battery (in coin cell format) with CNT/S cathodes and Li foil anodes. (a) Nyquist plots of the CNT/S-Single, CNT/S-Dual, and 2CNT/S-Dual electrodes from 1 MHz to 100 mHz at room temperature. (b) Rate performance of the CNT/S-Single, CNT/S-Dual, and 2CNT/S-Dual electrodes at different current densities. (c) Areal capacity at different current densities (charge/discharge rates) of the CNT/S-Single, CNT/S-Dual and the 2CNT/S-Dual electrodes. (d) Cycling performance and coulombic efficiency of the corresponding electrodes at  $\sim 0.5C$  charge/discharge rate for 200 cycles.

analysis. The EDS spectrum (inset of Figure 3c) and elemental mapping results confirm the uniform distribution of elements on the CNT film (Supporting Information Figure S6). The cross-sectional SEM images of the single side sulfur electrode and dual-side sulfur electrode with a thickness of approximately 22 and 40  $\mu\text{m}$ , respectively, indicate that the sulfur layer closely adheres to the surface of the CNT current collector films (Figure 3c, d) which is important to maintain electrical contact. X-ray diffraction (XRD) and Raman spectra of the pure CNT films and the sulfur-coated CNT films were also characterized (Supporting Information Figure S7–S8). Sharp diffraction peaks were observed in the sulfur-coated CNT film electrode, indicating the highly crystalline structure of sulfur (JCPDS card No. 08-0247). The diffraction peaks of the CNT film are also detectable at around 26 and 44° as shown in Supporting Information Figure S7.

**Li–S Battery Electrochemical Testing.** Electrochemical impedance spectroscopy (EIS) was used to analyze the electrochemical reaction kinetics to confirm whether or not the CNT film could provide good electron transport pathways. The tests were performed in the coin cell format with a Li metal foil as the counter-electrode. The Nyquist plots of CNT/S-Single, CNT/S-Dual, and 2CNT/S-Dual electrodes are qualitatively similar (Figure 4a) with a typical semicircle in the high-medium frequency region and an inclined line at low frequencies, which can be ascribed to the charge-transfer resistance  $R_{ct}$  and a mass-transfer process.<sup>27,28</sup> The value of  $R_{ct}$  for the CNT/S-Single electrode ( $\sim 110 \Omega$ ) is smaller than that of the CNT/S-Dual ( $\sim 127 \Omega$ ) and 2CNT/S-Dual electrodes ( $\sim 148 \Omega$ ). This is expected, since the increase of the sulfur loading

will also increase the electrochemical reaction resistance for the thicker electrodes. The rate capability, an important parameter for battery applications, was also investigated (Figure 4b). When the discharge current density was ramped up to  $\sim 3C$  ( $1C = 1675 \text{ mA g}^{-1}$ ), the 2CNT/S-Dual electrode (with a high sulfur loading of  $\sim 6.8 \text{ mg cm}^{-2}$ ) delivers a reversible capacity (normalized by the sulfur mass) of  $\sim 420 \text{ mAh g}^{-1}$ , which indicates the high rate capability of the electrode. When the current density was brought back down to  $\sim 0.5C$ , the performance of the CNT/S-Single, CNT/S-Dual, and 2CNT/S-Dual electrodes resume their original capacity of  $\sim 820$ ,  $\sim 780$ , and  $\sim 710 \text{ mAh g}^{-1}$ , exhibiting good stability. It should be noted that the CNT/S-Single electrode shows the best high rate performance due to its reduced sulfur loading and consequently superior electrical conductivity. This is consistent with the electrical conductivity (Supporting Information Figure S1) and EIS results (Figure 4a) shown previously. The areal capacities of these CNT/S electrodes were also calculated, as shown in Figure 4c. An exceptionally high areal capacity ( $\sim 7.2 \text{ mAh cm}^{-2}$  at 0.2C) with high sulfur loading ( $\sim 6.8 \text{ mg cm}^{-2}$ ) was obtained for the 2CNT/S-Dual electrode. Even when the current density was ramped up to 3C (high rate charge/discharge), the areal capacity was still maintained at  $\sim 2.8 \text{ mAh cm}^{-2}$ . Meanwhile, the electrodes also display good electrochemical cycling stability (Figure 4d). For example, the CNT/S-Single electrode showed an initial capacity of  $\sim 810 \text{ mAh g}^{-1}$  (at 0.5C) which drops to  $\sim 690 \text{ mAh g}^{-1}$  after 200 charge/discharge cycles. The average decay rate (at  $\sim 0.5C$ ) of the CNT/S-Single electrode is therefore  $\sim 0.11\%$  per cycle during the 200 cycles tested (Figure 4d).

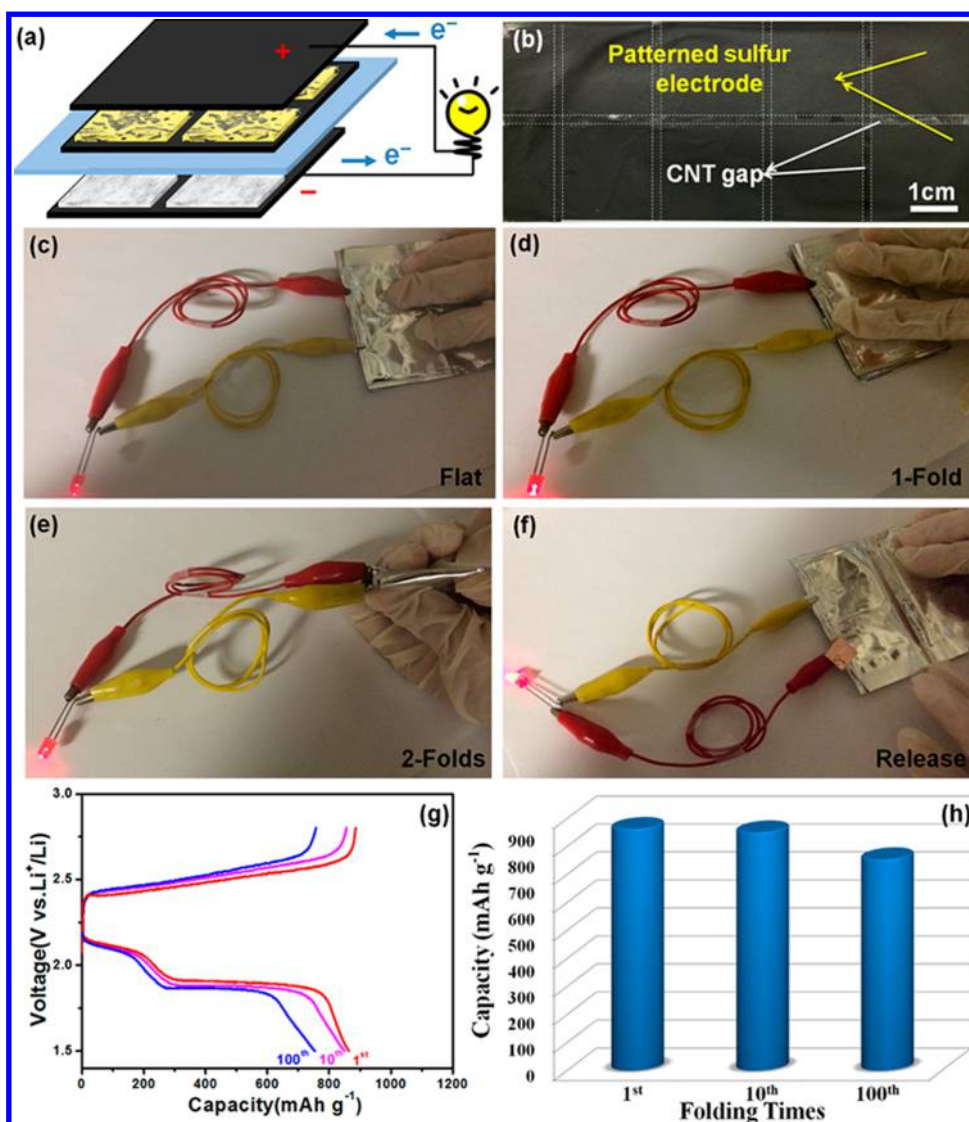


**Figure 5.** Pouch cell demonstration of foldable Li–S battery. (a) Schematic of the prototype foldable Li–S battery with the active materials (Li and S) patterned into the CNT current collector films in a checkerboard pattern. (b) Photograph showing patterning of sulfur into the CNT current collector. Similar patterning was also performed for the CNT–Li anode. (c–f) Qualitative demonstration of the insensitivity on the folding processes of the battery by checking the LED illumination. (g) Galvanostatic charge/discharge curves (charge/discharge rate =  $\sim 0.5C$ ) of the prototype foldable Li–S battery after 1, 10, and 100 folding/unfolding cycles. (f) Specific capacity (normalized by the total sulfur mass) of the foldable battery after 1, 10, and 100 folding/unfolding cycles at a charge/discharge rate of 0.5C.

To identify the electrochemical reactions, cyclic voltammogram (CV) measurements were carried out for the CNT/S–Single electrode in the range of 1.5–2.8 V for five cycles at a scan rate of  $0.1 \text{ mV s}^{-1}$  (Supporting Information Figure S9). During the first redox process, three cathodic peaks appeared at around 2.3 V (corresponding to the reduction of S to  $\text{Li}_2\text{S}_x$ ,  $4 < x < 8$ ), 2.1, and 2.0 V (corresponding to the reduction of  $\text{Li}_2\text{S}_4$  to lithium polysulfide intermediates and finally  $\text{Li}_2\text{S}_2/\text{Li}_2\text{S}$ ). In the subsequent anodic scan, one asymmetric broad oxidation peak is observed at around 2.4–2.5 V, which is attributed to the conversion of  $\text{Li}_2\text{S}$  to  $\text{Li}_2\text{S}_x$ ,  $2 < x < 8$  and S.<sup>26,29,30</sup> While the CV measurements elucidate the reaction chemistry, the electrochemical stability of the various electrodes was studied using

the galvanostatic charge–discharge cycling method shown previously in Figure 4d. We also used the galvanostatic charge–discharge method to study the performance of the pure CNT current collector (without any active materials). The results indicate that when the CNT film is utilized as the current collector in the Li–S battery (voltage range from 1.5 to 2.8 V (vs Li/Li<sup>+</sup>)) it does not make a significant contribution to the specific capacity (Supporting Information Figure S10). This is expected because the lithium ion intercalation and deintercalation process for the CNT film usually occurs below 1.0 V (vs Li/Li<sup>+</sup>).

To study the evolution of the lithium metal electrode in the Li–S battery, we carried out elemental mapping of the lithium metal surfaces in our CNT/S–Single,

**TABLE 1. Performance Parameters of Foldable Li–S Battery after 1, 10, and 100 Cycles of Folding<sup>a</sup>**

performance parameters	1st folding cycle	10th folding cycle	100th folding cycle
areal capacity (mAh cm <sup>-2</sup> )	3.11	3.06	2.71
gravimetric capacity (mAh g <sup>-1</sup> )	863.7	850.6	754.1
volumetric capacity (mAh L <sup>-1</sup> )	1.73 × 10 <sup>6</sup>	1.7 × 10 <sup>6</sup>	1.51 × 10 <sup>6</sup>
areal energy density (Wh cm <sup>-2</sup> )	2.7 × 10 <sup>-3</sup>	2.62 × 10 <sup>-3</sup>	2.3 × 10 <sup>-3</sup>
gravimetric energy density (Wh kg <sup>-1</sup> )	750	728	640
volumetric energy density (Wh L <sup>-1</sup> )	1080	1048	920
coulombic efficiency (%)	97.5	99.3	99.5

<sup>a</sup> The performance parameters listed include discharge capacity (areal, gravimetric, and volumetric), energy density (areal, gravimetric, and volumetric), and the coulombic efficiency. The gravimetric/volumetric energy densities are obtained by considering the mass/volume of the entire sulfur containing electrode (including the binder, conductive carbon black, CNT current collector films, and sulfur). The gravimetric/volumetric capacity is obtained by normalizing by the total sulfur mass/volume in the cell. The areal capacity is obtained by normalizing with respect to the electrode area.

CNT/S-Dual, and the 2CNT/S-Dual electrodes after 200 continuous cycles of charge and discharge and analyzed the anode's composition through EDS. It can be seen that the lithium metal surface is rougher with increasing sulfur content in the electrodes (Supporting Information Figure S11), which suggests greater polysulfide deposition on the lithium surface. This is also confirmed from the corresponding sulfur elemental mapping characterization. The increasing polysulfide content suggests that the cell with 2CNT/S-Dual electrode is expected to be less stable when compared to the CNT/S-Single electrode, which is consistent with the results in Figure 4d.

#### Demonstration of Foldable Li–S Battery Configuration by Patterning the Active Materials onto the CNT Current Collector.

For the tests in Figure 4, we used a Li metal foil as the anode material. A metallic Li foil cannot be folded without fracturing it. Therefore, to engineer a foldable anode that complements the foldable CNT/S cathode, we deposited Li on a CNT film in a checkerboard pattern (Figure 5a). The pattern was generated by using a template with square shaped openings to attach Li metal to the surface of the CNT current collector. The use of a checkerboard pattern means that the Li does not form a continuous film and the folding takes place predominantly in the pure CNT region (without Li). The Li deposited in the checkerboard pattern is therefore far less prone to delamination and fracture. To complement the anode, we also deposited the sulfur in the CNT/S-Single electrode in a checkerboard pattern using the same square shaped mask (Supporting Information Figure S12a,b). A schematic of the foldable Li–S full-cell (in the pouch cell format) is illustrated in Figure 5a, while Figure 5b shows the patterned CNT/S-Single electrode. This Li–S battery with the active materials patterned onto the CNT current collectors was used to power a light-emitting diode (LED). Figure 5c–f indicates that this patterned Li–S battery is insensitive to the folding processes and could be folded many times without any apparent change in the luminescence of the LED. The folding was performed along the axis defined by the checkerboard pattern in

Figure 5b. Further under the folded and the unfolded condition, the voltage of the Li–S battery remains very stable at ~2.4 V (Supporting Information Figure S12c,d), indicating that the folding does not degrade the output voltage of the battery. We anticipate that such folding along two orthogonal directions is suitable to meet the requirements of foldable electronics devices such as smart phones and tablet computers.

To evaluate the effect of folding on the electrochemical performance of the Li–S battery, we plot in Figure 5g the voltage profile of the prototype Li–S battery under the folded state after one, ten and hundred cycles of folding and unfolding. The mass loading of the patterned CNT/S-Single electrode used in this test was ~1.8 mg cm<sup>-2</sup> which increases to ~3.6 mg cm<sup>-2</sup> in the folded state (1-fold). The gravimetric capacity of the battery (normalized by the sulfur mass) is ~863.7 mAh g<sup>-1</sup> after one folding cycle and decreases to ~754.1 mAh g<sup>-1</sup> after 100 folding cycles, a decrease of ~12% (Figure 5h). Table 1 lists the key performance parameters of the foldable battery including the gravimetric, areal and volumetric capacities and energy densities as well as the coulombic efficiency. Note that the gravimetric/volumetric energy densities are obtained by considering the mass/volume of the sulfur containing electrode (including the binder, conductive carbon black, CNT current collector films, and sulfur). The areal capacities and energy densities of the foldable Li–S battery are significantly better than those of other foldable<sup>2–4</sup> and flexible<sup>14–18</sup> energy storage devices that have been reported in the literature. Table 1 also indicates that the various performance parameters of the Li–S battery are not significantly degraded over 100 folding and unfolding cycles. We attribute this to the deposition of the active materials (Li, S) onto the foldable carbon nanotube current collectors in a checkerboard pattern, making them far less prone to delamination and fracture.

## CONCLUSIONS

In summary, we report a foldable Li–S battery with superior areal capacity and energy density when

compared to traditional foldable energy storage devices. The device is foldable because it utilizes super-elastic CNT films as current collectors with the active material patterned into the current collector in a checkerboard pattern. The manufacturing processes for the foldable Li–S battery, including the slurry mixing, patterned coating, and packaging are straightforward without the need for any complicated equipment and compatible with mainstream industrial processing. The CNT current collectors can also

be produced in a scalable manner using FC-CVD. The reliability of the sealing of the liquid electrolyte in the pouch cell will need to be investigated, and perhaps the use of a solid electrolyte may be more desirable for practical applications. These issues should be addressed in future work, and we expect that this study will provide new impetus to both academia and industry to explore the development of Li–S batteries in flexible and foldable energy storage devices.

## METHODS

**Preparation of CNT Film.** The CNT films were prepared by methanol mediated floating catalyst chemical vapor deposition<sup>19</sup> at  $\sim 1150$  °C. Large area CNT films ( $\sim 1000$  cm<sup>2</sup>) could be produced with the area density of around 0.6–0.8 mg cm<sup>-2</sup> and a thickness of  $\sim 3$   $\mu$ m.

**Electrode Preparation.** A homogeneous sulfur-containing slurry (70 wt % commercial sulfur powder as active material, 20 wt % carbon black as conductive agent, and 10 wt % PVDF as binder dissolved in the *N*-methyl-2-pyrrolidone) was spread on CNT film by the doctor blade. Then, it was dried in a vacuum drying oven at  $\sim 60$  °C for  $\sim 12$  h. For the patterned sulfur electrodes, the template (or mask) was placed on the surface of CNT film before coating sulfur-containing slurry (Supporting Information Figure S12a). The corresponding patterned anode was prepared by adhering Li squares on the CNT film using the mask. For the dual-side sulfur coated electrodes, the second coating was carried out when the former coating has dried. The mass loading of sulfur was  $\sim 1.8$ ,  $\sim 3.4$ , and  $\sim 6.8$  mg cm<sup>-2</sup> for the CNT/S-Single, CNT/S-Dual, and 2CNT/S-Dual electrodes resulting in sulfur contents of  $\sim 45\%$ ,  $\sim 49\%$ , and  $\sim 52\%$ , respectively (based on the total mass of the electrode including CNT film, conductive additives and binders).

**Material Characterization.** The structure of the materials was investigated by SEM (Carl Zeiss Supra field-emission scanning electron microscope). EDS was used for collecting elemental signals and mapping. TEM was carried out by using a JEOL JEM-2010 instrument. XRD was conducted with a PANalytical diffractometer (Cu K $\alpha$ ). Raman spectroscopy was performed by the Witec Alpha 300R confocal Raman imaging system.

**Electrochemical Measurements.** Stainless steel coin cells (2032-type) were used to assemble test cells, and Celgard 2340 polypropylene membrane was used as the separator. For the Li–S foldable pouch battery, Al and Cu strips as the electrode tabs, were attached to the CNT current collector films on the cathode and anode side, respectively. Sealing was achieved by means of a heat sealer (see Supporting Information Figure S12b). The electrolyte that was utilized was  $\sim 1.0$  M lithium bis-trifluoromethanesulfonylimide in 1,3-dioxolane and 1,2-dimethoxyethane (1:1 by volume) with 0.1 mol L<sup>-1</sup> LiNO<sub>3</sub> additive. The addition of LiNO<sub>3</sub> promotes the formation of a stable passivation film on the lithium anode surface. This is beneficial to prevent the reduction products depositing on the metallic lithium surface and also the further reaction of lithium with soluble polysulfide in the electrolyte. All cells were assembled inside a glovebox (MBraun Labstar). Galvanostatic charge–discharge cycles were performed using an Arbin BT2000 battery instrument at various current densities over the voltage range from 1.5 to 2.8 V (vs. Li/Li<sup>+</sup>). Cyclic voltammogram (CV) and electrochemical impedance spectroscopy (EIS) data were collected using a Gamry Instruments potentiostat in the voltage range of 1.5–2.8 V (vs. Li<sup>+</sup>/Li) at a scan rate of 0.1 mV s<sup>-1</sup> and in the frequency range of 1 MHz to 100 mHz at room temperature.

**Theoretical Calculations.** Reactive force field interatomic potential (ReaxFF) is applied in LAMMPS<sup>31</sup> to capture the bending behavior of carbon atoms in our system. This potential is a bond-order-based potential in molecular dynamics simulation

and could accurately describe not only the bonded interaction, for example, chemical bonds, valence angles, and torsion angles between carbon atoms in one DWCNT, but also nonbonded interactions, such as van der Waals force between the carbon atoms of different DWCNTs. It has been used in numerous studies<sup>31–33</sup> of mechanical deformation of CNTs. We built three models of DWCNT with diameter of 1.6 nm for the outer wall and 1.2 nm for the inner wall. Although these dimensions are different from experiment, the physical reason for the folding process should be the same. For the cross-linking configuration, the lengths of the bending and cross-linked DWCNT were chosen as 140 and 28 nm, respectively. In order to simulate conditions analogous to experiments in which individual CNTs in a nanotube bundle would experience bending at multiple points, periodic boundary conditions were assumed. One simulation with fixed boundary on the top and bottom along *y*-axis was also conducted, and results did not show appreciable difference from the periodic case. All the simulations were performed at constant temperature of 300 K with isothermal–isobaric relaxation process (NPT). Atomeye<sup>34</sup> was used to capture the strain distribution.

**Conflict of Interest:** The authors declare no competing financial interest.

**Acknowledgment.** N.K. acknowledges funding support from the United States National Science Foundation (Award Numbers: 1234641 and 1435783). N.K. also acknowledges support from the John A. Clark and Edward T. Crossan endowed chair professorship at the Rensselaer Polytechnic Institute. This work was also supported by the International Collaborative Energy Technology R&D Program of the Korea Institute of Energy Technology Evaluation and Planning (KETEP), granted financial resource from the Ministry of Trade, Industry & Energy, Republic of Korea (No. 20128510010050). Z.P.W. acknowledges funding support from the National Natural Science Foundation of China (Awards 51202095 and 51264010). C.V.S. and H.S. acknowledge support from Natural Science and Engineering Research Council (NSERC) of Canada for funding, and Compute Canada facilities SciNet and SharcNet for computational resources.

**Supporting Information Available:** The Supporting Information is available free of charge on the ACS Publications website at DOI: 10.1021/acs.nano.5b05068.

CNT-sulfur film electrical conductivity measurements, details of MD simulation setup and additional simulation results, EDS elemental mapping of CNT-sulfur film, XRD and Raman characterization of CNT and CNT-sulfur films, cyclic voltammogram (CV) scans, electrochemical characterization of pure CNT film, postcycling SEM and EDS characterization of the lithium metal electrode, fabrication of patterned electrodes, and output voltage of Li–S battery in the unfolded and folded condition (PDF)

## REFERENCES AND NOTES

- Zhou, G.; Li, F.; Cheng, H.-M. Progress in Flexible Lithium Batteries and Future Prospects. *Energy Environ. Sci.* **2014**, *7*, 1307–1338.

2. Hu, J. W.; Wu, Z. P.; Zhong, S. W.; Zhang, W. B.; Suresh, S.; Mehta, A.; Koratkar, N. Folding Insensitive, High Energy Density Lithium-Ion Battery Featuring Carbon Nanotube Current Collectors. *Carbon* **2015**, *87*, 292–298.
3. Song, Z.; Ma, T.; Tang, R.; Cheng, Q.; Wang, X.; Krishnaraju, D.; Panat, R.; Chan, C. K.; Yu, H.; Jiang, H. Origami Lithium-Ion Batteries. *Nat. Commun.* **2014**, *5*, 3140.
4. Cheng, Q.; Song, Z.; Ma, T.; Smith, B. B.; Tang, R.; Yu, H.; Jiang, H.; Chan, C. K. Folding Paper-Based Lithium-Ion Batteries for Higher Areal Energy Densities. *Nano Lett.* **2013**, *13*, 4969–4974.
5. Xu, P.; Gu, T.; Cao, Z.; Wei, B.; Yu, J.; Li, F.; Byun, J.-H.; Lu, W.; Li, Q.; Chou, T.-W. Carbon Nanotube Fiber Based Stretchable Wire-Shaped Supercapacitors. *Adv. Energy Mater.* **2014**, *4*, 1300759.
6. Manthiram, A.; Fu, Y.; Su, Y.-S. Challenges and Prospects of Lithium–Sulfur Batteries. *Acc. Chem. Res.* **2013**, *46*, 1125–1134.
7. Mukherjee, R.; Thomas, A. V.; Datta, D.; Singh, E.; Li, J.; Eksik, O.; Shenoy, V. B.; Koratkar, N. Defect-Induced Plating of Lithium Metal within Porous Graphene Networks. *Nat. Commun.* **2014**, *5*, 3710.
8. Zhong, J.; Yang, Z.; Mukherjee, R.; Varghese Thomas, A.; Zhu, K.; Sun, P.; Lian, J.; Zhu, H.; Koratkar, N. Carbon Nanotube Sponges as Conductive Networks for Supercapacitor Devices. *Nano Energy* **2013**, *2*, 1025–1030.
9. Pantano, A.; Boyce, M. C.; Parks, D. M. Nonlinear Structural Mechanics Based Modeling of Carbon Nanotube Deformation. *Phys. Rev. Lett.* **2003**, *91*, 145504.
10. Iijima, S.; Brabec, C.; Maiti, A.; Bernholc, J. Structural Flexibility of Carbon Nanotubes. *J. Chem. Phys.* **1996**, *104*, 2089–2092.
11. Zhou, G.; Li, L.; Ma, C.; Wang, S.; Shi, Y.; Koratkar, N.; Ren, W.; Li, F.; Cheng, H.-M. A Graphene Foam Electrode with High Sulfur Loading for Flexible and High Energy Li-S Batteries. *Nano Energy* **2015**, *11*, 356–365.
12. Zhu, L.; Peng, H.-J.; Liang, J.; Huang, J.-Q.; Chen, C.-M.; Guo, X.; Zhu, W.; Li, P.; Zhang, Q. Interconnected Carbon Nanotube/Graphene Nanosphere Scaffolds as Free-Standing Paper Electrode for High-Rate and Ultra-Stable Lithium–Sulfur Batteries. *Nano Energy* **2015**, *11*, 746–755.
13. Qie, L.; Manthiram, A. A Facile Layer-by-Layer Approach for High-Areal-Capacity Sulfur Cathodes. *Adv. Mater.* **2015**, *27*, 1694–1700.
14. Kwon, Y. H.; Woo, S.-W.; Jung, H.-R.; Yu, H. K.; Kim, K.; Oh, B. H.; Ahn, S.; Lee, S.-Y.; Song, S.-W.; Cho, J. *et al.* Cable-Type Flexible Lithium Ion Battery Based on Hollow Multi-Helix Electrodes. *Adv. Mater.* **2012**, *24*, 5192–5197.
15. Gaikwad, A. M.; Khau, B. V.; Davies, G.; Hertzberg, B.; Steingart, D. A.; Arias, A. C. A High Areal Capacity Flexible Lithium-Ion Battery with a Strain-Compliant Design. *Adv. Energy Mater.* **2015**, *5*, 1401389.
16. Weng, W.; Sun, Q.; Zhang, Y.; He, S.; Wu, Q.; Deng, J.; Fang, X.; Guan, G.; Ren, J.; Peng, H. A Gum-Like Lithium-Ion Battery Based on a Novel Arched Structure. *Adv. Mater.* **2015**, *27*, 1363–1369.
17. Kim, J.-S.; Ko, D.; Yoo, D.-J.; Jung, D. S.; Yavuz, C. T.; Kim, N.-I.; Choi, I.-S.; Song, J. Y.; Choi, J. W. A Half Millimeter Thick Coplanar Flexible Battery with Wireless Recharging Capability. *Nano Lett.* **2015**, *15*, 2350–2357.
18. Xu, S.; Zhang, Y.; Cho, J.; Lee, J.; Huang, X.; Jia, L.; Fan, J. A.; Su, Y.; Su, J.; Zhang, H. *et al.* Stretchable Batteries with Self-Similar Serpentine Interconnects and Integrated Wireless Recharging Systems. *Nat. Commun.* **2013**, *4*, 1543.
19. Wu, Z.; Xu, Q.; Wang, J.; Ma, J. Preparation of Large Area Double-Walled Carbon Nanotube Macro-Films with Self-Cleaning Properties. *J. Mater. Sci. Technol.* **2010**, *26*, 20–26.
20. Braithwaite, J. W.; Gonzales, A.; Nagasubramanian, G.; Lucero, S. J.; Peebles, D. E.; Ohlhausen, J. A.; Cieslak, W. R. Corrosion of Lithium-Ion Battery Current Collectors. *J. Electrochem. Soc.* **1999**, *146*, 448–456.
21. Shima, H. Buckling of Carbon Nanotubes: A State of the Art Review. *Materials* **2012**, *5*, 47–84.
22. Feliciano, J.; Tang, C.; Zhang, Y.; Chen, C. Aspect Ratio Dependent Buckling Mode Transition in Single-Walled Carbon Nanotubes under Compression. *J. Appl. Phys.* **2011**, *109*, 084323.
23. Hertel, T.; Walkup, R. E.; Avouris, P. Deformation of Carbon Nanotubes by Surface Van Der Waals Forces. *Phys. Rev. B: Condens. Matter Mater. Phys.* **1998**, *58*, 13870–13873.
24. Arroyo, M.; Belytschko, T. Nonlinear Mechanical Response and Rippling of Thick Multiwalled Carbon Nanotubes. *Phys. Rev. Lett.* **2003**, *91*, 215505.
25. Su, Y.-S.; Manthiram, A. A New Approach to Improve Cycle Performance of Rechargeable Lithium-Sulfur Batteries by Inserting a Free-Standing MWCNT Interlayer. *Chem. Commun.* **2012**, *48*, 8817–8819.
26. Zhou, G. M.; Pei, S.; Li, L.; Wang, D.-W.; Wang, S.; Huang, K.; Yin, L.-C.; Li, F.; Cheng, H.-M. A Graphene–Pure-Sulfur Sandwich Structure for Ultrafast, Long-Life Lithium–Sulfur Batteries. *Adv. Mater.* **2014**, *26*, 625–631.
27. Zhou, G.; Li, L.; Wang, D.-W.; Shan, X.-Y.; Pei, S.; Li, F.; Cheng, X.-Y. A Flexible Sulfur-Graphene-Polypropylene Separator Integrated Electrode for Advanced Li–S Batteries. *Adv. Mater.* **2015**, *27*, 641–647.
28. Reddy, M. V.; Yu, T.; Sow, C. H.; Shen, Z. X.; Lim, C. T.; Subba Rao, G. V.; Chowdari, B. V. R.  $\alpha$ -Fe<sub>2</sub>O<sub>3</sub> Nanoflakes as an Anode Material for Li-Ion Batteries. *Adv. Funct. Mater.* **2007**, *17*, 2792–2799.
29. Zhao, M.-Q.; Zhang, Q.; Huang, J.-Q.; Tian, G.-L.; Nie, J.-Q.; Peng, H.-J.; Wei, F. Unstacked Double-Layer Templated Graphene for High-Rate Lithium–Sulphur Batteries. *Nat. Commun.* **2014**, *5*, 3410.
30. Zhou, G.; Wang, D.-W.; Li, F.; Hou, P.-X.; Yin, L.; Liu, C.; Lu, G. Q.; Gentle, I. R.; Cheng, H.-M. A Flexible Nanostructured Sulphur-Carbon Nanotube Cathode with High Rate Performance for Li-S Batteries. *Energy Environ. Sci.* **2012**, *5*, 8901–8906.
31. Plimpton, S. Fast Parallel Algorithms for Short-Range Molecular Dynamics. *J. Comput. Phys.* **1995**, *117*, 1–19.
32. Cranford, S. W.; Buehler, M. J. Mechanical Properties of Graphyne. *Carbon* **2011**, *49*, 4111–4121.
33. Zandiatashbar, A.; Lee, G.-H.; An, S. J.; Lee, S.; Mathew, N.; Terrones, M.; Hayashi, T.; Picu, C. R.; Hone, J.; Koratkar, N. Effect of Defects on the Intrinsic Strength and Stiffness of Graphene. *Nat. Commun.* **2014**, *5*, 3186.
34. Li, J. Atomeye: An Efficient Atomistic Configuration Viewer. *Model. Simul. Mater. Sci. Eng.* **2003**, *11*, 173.